

**Crater functions for compound materials: a route to parameter  
estimation in coupled-PDE models of ion bombardment**

Scott A. Norris

*Southern Methodist University*

*Department of Mathematics*

*3200 Dyer Street*

*Dallas, TX, 75275*

Juha Samela, Matias Vestberg, and Kai Nordlund

*University of Helsinki*

*Department of Physics*

*PB 43, 00014 University of Helsinki*

*Finland*

Michael J. Aziz

*Harvard University*

*School of Engineering and Applied Sciences*

*29 Oxford Street*

*Boston, MA 02138*

## Abstract

During the ion bombardment of targets containing multiple component species, highly-ordered arrays of nanostructures are sometimes observed. Models incorporating coupled partial differential equations, describing both morphological and chemical evolution, seem to offer the most promise of explaining these observations. However, these models contain many unknown parameters, which must satisfy specific conditions in order to explain observed behavior. The lack of knowledge of these parameters is therefore an important barrier to the comparison of theory with experiment. Here, by adapting the recent theory of “crater functions” to the case of binary materials, we develop a generic framework in which many of the parameters of such models can be estimated using the results of molecular dynamics simulations.

As a demonstration, we apply our framework to the recent theory of Bradley and Shipman, for the case of Ar-irradiated GaSb, in which ordered patterns were first observed. In contrast to the requirements therein that sputtered atoms form the dominant component of the collision cascade, and that preferential redistribution play an important stabilizing role, we find instead that the redistributed atoms dominate the collision cascade, and that preferential redistribution appears negligible. Hence, the actual estimated parameters for this system do not seem to satisfy the requirements imposed by current theory, motivating the consideration of other potential pattern-forming mechanisms.

## I. INTRODUCTION

The irradiation of flat surfaces by low-energy ions can lead to the emergence of ordered arrays of nanoscale surface features [1], and offers the potential to assist in the fabrication of nanostructured devices with regular structure [2]. Initially observed on a wide variety of target materials [3–5], careful experimental investigation has led to a growing consensus that these structures only appear during the irradiation of binary materials, or environments in which one or more materials is simultaneously co-deposited during the irradiation process [6–11]. This consensus has motivated a number of theoretical treatments of irradiated two-component materials, in which a coupled pair of partial differential equations simultaneously track the evolution of both the morphology and the concentration. Extending the earlier work of Shenoy, Chan, and Chason [12], Bradley and Shipman (BS) have recently introduced such a theory exhibiting the first physically-grounded explanation for the strong ordering of the observed nanostructures [13, 14]. This result has sparked great interest, inspiring additional studies on normal-incidence irradiation of two-component materials [15], including a variant where the second material is not originally present, but instead co-deposited simultaneously with the ion irradiation [16], and a similar framework for the study of ion-assisted deposition, where both materials are deposited along with the ions, and the deposition rate exceeds the sputtering rate [17].

Despite their successes, however, the models in this family face some important open questions. In particular, they contain many competing physical effects, represented by a large number of parameters whose values are difficult to estimate experimentally, and are thus so far undetermined. Although each theory seems reasonably able to explain experimental observations for some region of parameter space, it is unknown whether the various systems actually have parameters within those regions. The lack of parameter estimates is therefore an important barrier to the quantitative comparison of theory to experiment. In this context, we will here develop a framework for the estimation of several of these parameters by means of molecular dynamics simulations, by extending the theory of “crater functions” [18, 19] to the case of binary materials.

We will begin in Section II with a necessary, brief review of the key features of coupled-PDE theories, which have a common mathematical structure and some generic stability

properties. Then, in Section III, we perform the first half of our task: we show how a generalization of crater function theory, as in the case of pure materials, allows the extraction of several terms of a continuum equation for the evolution of the surface height, in terms of moments of the crater function associated with simulations of single-ion impact. The second half is to compare that equation with the corresponding equation in any particular coupled-PDE model, by which one can in principle extract several underlying parameters of the model, which in turn allow estimates of the coefficients present in the PDEs.

Finally, in Section IV, we provide a lengthy demonstration of our approach for the Bradley-Shipman theory itself [13, 14], as applied to the long-studied  $\text{Ar}^+ \rightarrow \text{GaSb}$  system [1, 20, 21]. Estimating four important parameters for this theory using the framework developed in Section III, our principal findings are that the destabilizing effect of sputtered atoms [22] continues to be overwhelmed by the stabilizing effect of redistributed atoms [23, 24], and that the species-dependent redistribution seems to be negligible. Both of these observations are contrary to the requirements for ordered pattern formation imposed by the Bradley-Shipman model, and suggest that additional or alternate physical mechanisms may be necessary to explain this phenomena.

## II. REVIEW OF EXISTING THEORY: MODELS AND STABILITY ANALYSIS

We begin by briefly summarizing a recent class of models including contributions from Shenoy, Chan, and Chason [12], Bradley and Shipman [13, 14], Bradley [15, 16], and Abrasonis and Morowetz [17] for various irradiation regimes involving two target species. Because extensive analysis of this class of models exists elsewhere, both in the just-cited works, and in general [25], we will be as brief as possible. However, because our aim is to test specific aspects of these theories, we must include those results that are directly relevant to the molecular dynamics simulations we perform later.

### A. Models

The models cited above all consider the normal-incidence irradiation of an initially flat target which contains two components in one of three ways: (a) the target itself is a binary material [13–15], (b) the target is pure, but a second material is co-deposited

during sputtering [16], or (c) two materials are co-deposited at a rate that exceeds the net sputter rate [17] (termed Ion Beam Assisted Deposition or IBAD). In any of these cases, one tracks the evolution of a height field  $z = h(x, y, t)$  describing the irradiated surface, and concentration fields  $c_A(x, y, t)$  and  $c_B(x, y, t)$  of two components  $A$  and  $B$ . Under the effects of preferential sputtering, a steady state is reached in which the material is receding (or advancing, for IBAD) with constant velocity  $v_0$  and constant surface concentrations  $c_{A,0}$  and  $c_{B,0}$  of  $A$  and  $B$  atoms, respectively. The stability of this steady state is then investigated by introducing perturbations of the form

$$\begin{aligned} h &= -v_0 t + u(x, y, t) \\ c_A &= c_{A,0} + \phi(x, y, t) \\ c_B &= c_{B,0} + (1 - \phi)(x, y, t) \end{aligned} \tag{1}$$

where  $u(x, y, t)$  describes a small perturbation to the height field, and  $\phi(x, y, t)$  describes a small perturbation to the concentration field of species  $A$ . After significant modeling of various physical effects during ion irradiation, each of Refs.[13–17] obtains linearized equations for the evolution of  $u$  and  $\phi$  of the form

$$\frac{\partial u}{\partial t} = -A\phi + B\nabla^2\phi + C\nabla^2u - D\nabla^4u \tag{2}$$

$$\frac{\partial \phi}{\partial t} = -A'\phi + B'\nabla^2\phi + C'\nabla^2u - D'\nabla^4u. \tag{3}$$

The exact meaning of the coefficients varies among the cited models, but in general the following interpretations may be provided. In Eq. (2) describing the height field: the term  $-A\phi$  describes the concentration dependence of the net erosion rate, so that if  $A > 0$  then increasing the concentration of species  $A$  increases the sputter yield [12]; the term  $B\nabla^2\phi$  describes a *net* mass flux along concentration gradients caused by unequal diffusivities between the components; the term  $C\nabla^2u$  captures the net effects of both curvature dependent sputtering [22] and mass redistribution [23] (and also stress [26–28], which will however be neglected here); the term  $-D\nabla^4u$  (with  $D > 0$  by definition) describes many kinds of surface relaxation including surface diffusion [22, 29] and surface-confined viscous flow [30, 31], and regularizes the height dependence in the case that  $C$  is negative. In Eq.(3) describing the concentration field: the term  $-A'\phi$  (with  $A' > 0$  by definition)

describes the continual resupply of material into the irradiated film at some reference concentration of either the bulk (in the regime of erosion) or the vapor (in the regime of growth), which serves to damp perturbations away from this concentration; the term  $B'\nabla^2\phi$  describes simple Fickian diffusion; the term  $C'\nabla^2u$  describes species-dependent redistribution [13], and the term  $-D'\nabla^4u$  would describe preferential migration away from regions of high curvature, due to differing atomic mobilities.

## B. Generic Stability Analysis

To determine the presence or absence of an instability, it is sufficient to consider a one-dimensional perturbation, because of the isotropic nature of normal-incidence irradiation. Without loss of generality, we may orient this instability in the  $x$ -coordinate direction, giving

$$\begin{bmatrix} u(x, t) \\ \phi(x, t) \end{bmatrix} = \begin{bmatrix} u_1 \\ \phi_1 \end{bmatrix} e^{ikx + \sigma t}, \quad (4)$$

where  $k$  is the wavenumber of the perturbation,  $\sigma(k)$  the (wavenumber-dependent) growth rate of that perturbation, and  $u_1$  and  $\phi_1$  are undetermined constants describing the relative phases and magnitudes of the height and concentration modulations. Inserting the ansatz (4) into the linearized equations (2)-(3), we obtain, in matrix form,

$$\begin{bmatrix} \sigma + Ck^2 + Dk^4 & A + Bk^2 \\ C'k^2 + D'k^4 & \sigma + A' + B'k^2 \end{bmatrix} \begin{bmatrix} u_1 \\ \phi_1 \end{bmatrix} = \mathbf{0}. \quad (5)$$

For a solution  $[u_1, \phi_1]^T$  of this equation, the determinant of the matrix must be zero, giving a the dispersion relation  $\sigma(k)$  in the quadratic form

$$\sigma^2 + \tau\sigma + \Delta = 0, \quad (6)$$

where  $\tau(k)$  and  $\Delta(k)$  are respectively the trace and determinant of (5) when  $\sigma = 0$ :

$$\tau(k) = A' + (C + B')k^2 + Dk^4 \quad (7)$$

$$\Delta(k) = (CA' - AC')k^2 + (CB' - C'B + DA' - D'A)k^4 + (DB' - D'B)k^6. \quad (8)$$

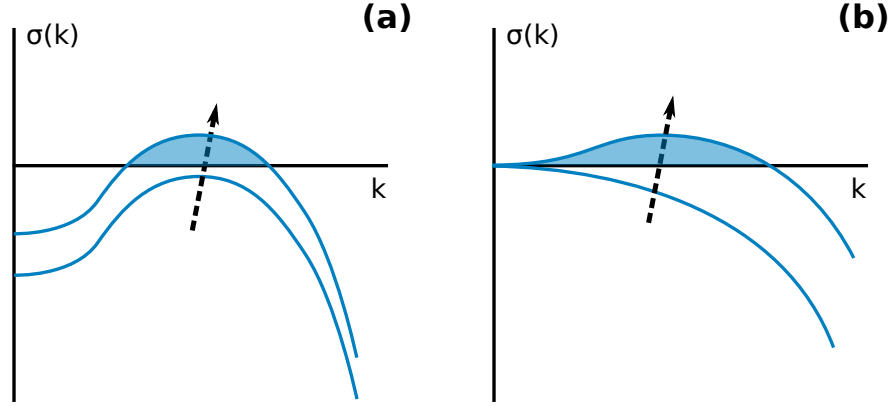


Figure 1. (a) A finite-wavelength instability, in which a narrow band of unstable wavenumbers emerges, bounded above and below by stable wavenumbers. Systems with linear instabilities of this kind generically exhibit some kind of ordered pattern. (b) A long-wavelength instability, in which all wavenumbers below a critical value are unstable. Systems with linear instabilities of this kind generically exhibit roughening and coarsening.

For the purpose of identifying stability properties, it is sufficient to consider only the root associated with the '+' sign in the quadratic formula which, following common practice, is denoted  $\sigma_+(k)$ :

$$\sigma_+(k) = \frac{1}{2} \left( -\tau + \sqrt{\tau^2 - 4\Delta} \right). \quad (9)$$

This gives the growth rate of the faster-growing solution when the discriminant is positive.

### C. Discussion: Pattern Formation and Coefficient Values

The expected behavior of an initially-flat surface is determined by the dispersion relation  $\sigma_+(k)$ . Wavenumbers  $k$  for which  $\sigma_+(k) < 0$  are stable and decay over time, while those  $k$  for which  $\sigma_+(k) > 0$  are unstable and grow over time. Provided at least some wavenumbers are unstable, then some kind of structure emerges on the irradiated surface. However, the nature and evolution of this structure depends strongly on the nature of  $\sigma_+(k)$ , as extensively discussed in Refs. [25]. In particular, if the unstable wavenumbers exist only in a narrow band, surrounded on both sides by stable wavenumbers, then the limited range of unstable wavelengths drives the system into a relatively well-ordered con-

figuration that preserves its characteristic size over time (Figure 1a). On the other hand, if all wavenumbers below a critical value are unstable, then the system tends to roughen and coarsen over time, as the slower-growing but energetically-favorable longer wavelengths take over from the initial instability (Figure 1b).

Based on these considerations, it is clear that a key determinant of the observed pattern is the stability of the longwaves: if a system is observed to exhibit well-ordered patterns in the linear regime, it must be true that the longwaves are linearly stable. From Eqs. (7)-(9) in the limit as  $k \rightarrow 0$ , we can easily find that for small values of  $k$

$$\lim_{k \rightarrow 0} \sigma_+(k) \approx -\frac{1}{A'} (A'C - C'A) k^2 + \mathcal{O}(k^4). \quad (10)$$

Hence, any system with well-ordered patterns must satisfy the requirement

$$A'C - C'A > 0; \quad (11)$$

this provides a tangible and concrete test for the comparison of theory with experiment. We see that this important predictor of qualitative system behavior depends on no less than four of the unknown theoretical parameters, which highlights the importance of finding ways to produce estimates of these coefficients. More intriguingly, we see from the definitions above that each of these parameters is associated in some way with the effect of ion impacts, which suggests the possibility of estimating these parameters via molecular dynamics.

### III. COEFFICIENT ESTIMATION VIA MOLECULAR DYNAMICS: CRATER FUNCTIONS FOR COMPOUND MATERIALS

We now develop a framework in which the results of MD simulation may be connected to the coefficients of Eqs.(2)-(3). To this end, we will generalize the “crater function” theory for surface morphology evolution [18, 19] - which extracts certain PDE terms directly from molecular dynamics simulations - to the case of a multi-component material. Because the generalization is straightforward, we will rely heavily on the referenced works, and present only the differences in the present approach.

We begin by taking the “crater function”  $\Delta h(x, y; \theta)$ , describing the average change in surface morphology to a flat surface due to the impact of a single ion at the origin, and



splitting it into four parts:

$$\Delta h(x, y; \theta, c_A, c_B) = \Delta h_A^{\text{eros.}} + \Delta h_B^{\text{eros.}} + \Delta h_A^{\text{redist.}} + \Delta h_B^{\text{redist.}}. \quad (12)$$

This merely states that the change in surface topography due to a single ion impact is the superposition of effects due to both eroded and redistributed atoms, of both species A and species B. A central benefit of this approach is that any subsequent analytical treatment of  $\Delta h$  treats all these effects simultaneously. Therefore, because the multi-scale analysis of Ref.[18] (and a simplified approximation for flat targets in Ref.[19]) has already been performed for a general  $\Delta h$ , all the resulting PDE terms therein can be similarly decomposed into contributions of the same four types.

To estimate the components in Eq.(12) from a molecular dynamics simulation, we follow Ref.[18] by assuming that all displacements within the bulk are immediately projected to the surface to cause a change in the surface profile, which can then be approximated by placing delta functions at the initial and final position of each atom. Using Eqs.(46) and (48) of Ref.[18] as a template, we define

$$\begin{aligned} \Delta h_A^{\text{eros.}} &= -\Omega_A \sum_i \delta(\mathbf{x}_i^I) \\ \Delta h_B^{\text{eros.}} &= -\Omega_B \sum_j \delta(\mathbf{x}_j^I) \\ \Delta h_A^{\text{redist.}} &= \Omega_A \sum_k \delta(\mathbf{x}_k^F) - \delta(\mathbf{x}_k^I) \\ \Delta h_B^{\text{redist.}} &= \Omega_B \sum_l \delta(\mathbf{x}_l^F) - \delta(\mathbf{x}_l^I) \end{aligned} \quad (13)$$

where the  $\Omega$  denote atomic volumes,  $i, j$  denote sputtered  $A, B$  atoms,  $k, l$  denote displaced  $A, B$  atoms, and  $\mathbf{x}^I$  and  $\mathbf{x}^F$  denote initial and final target atom positions associated with an ion impact.

A central result of Refs.[18, 19] is that morphology evolution depends only on the moments of the crater function (12). When the crater function is integrated to obtain these moments, each moment automatically contains associated contributions of each type. Following Eqs.(47) and (49) of Ref.[18] by directly integrating the components in Eq.13, we

obtain the moments via

$$\begin{aligned}
M_A^{(0)} &= \int \Delta h_A^{\text{eros.}} dA &= -\Omega_A \sum_i 1 \\
M_B^{(0)} &= \int \Delta h_B^{\text{eros.}} dA &= -\Omega_B \sum_j 1 \\
M_{A,\text{eros.}}^{(1)} &= \int \mathbf{x} \Delta h_A^{\text{eros.}} dA &= -\Omega_A \sum_i \mathbf{x}_i^{\text{I}} \\
M_{B,\text{eros.}}^{(1)} &= \int \mathbf{x} \Delta h_B^{\text{eros.}} dA &= -\Omega_B \sum_j \mathbf{x}_j^{\text{I}} \\
M_{A,\text{redist.}}^{(1)} &= \int \mathbf{x} \Delta h_A^{\text{redist.}} dA &= \Omega_A \sum_k (\mathbf{x}_k^{\text{F}} - \mathbf{x}_k^{\text{I}}) \\
M_{B,\text{redist.}}^{(1)} &= \int \mathbf{x} \Delta h_B^{\text{redist.}} dA &= \Omega_B \sum_l (\mathbf{x}_l^{\text{F}} - \mathbf{x}_l^{\text{I}})
\end{aligned} \tag{14}$$

(note that the zeroth moment has no redistributive part). Although additional moments exist and contribute, in principle, to the dynamics of the surface, no theory to date incorporates these effects; as our present goal is to estimate the coefficients of existing theories, we will not consider higher moments here.

Finally, following a multi-scale analysis, these contributions to the moments produce associated terms in the governing equation for the height field

$$\begin{aligned}
h_t &\approx (Y^A + Y^B) \\
&+ \left( S_X^{A,\text{eros.}} + S_X^{B,\text{eros.}} + S_X^{A,\text{redist.}} + S_X^{B,\text{redist.}} \right) h_{xx} \\
&+ \left( S_Y^{A,\text{eros.}} + S_Y^{B,\text{eros.}} + S_Y^{A,\text{redist.}} + S_Y^{B,\text{redist.}} \right) h_{yy}
\end{aligned} \tag{15}$$

with definitions given by Eq.(4) of Ref.[19]

$$\begin{aligned}
Y^Z(\theta, c_i) &= \left[ I_0 \cos(\theta) M_Z^{(0)}(\theta, c_i) \right] \\
S_X^{Z,\text{type}}(\theta, c_i) &= \frac{\partial}{\partial \theta} \left[ I_0 \cos(\theta) M_{Z,\text{type}}^{(1)}(\theta, c_i) \right] , \\
S_Y^{Z,\text{type}}(\theta, c_i) &= \left[ I_0 \cos(\theta) \cot(\theta) M_{Z,\text{type}}^{(1)}(\theta, c_i) \right]
\end{aligned} \tag{16}$$

where  $Z$  is either  $A$  or  $B$ , 'type' is either 'eros.' or 'redist.', and  $I_0$  is the flux through a plane perpendicular to the beam (see Section IVE for further comments on these formulas).

Equation (15) completely describes the response of the surface to the effects of sputtered atoms (via the base yield terms  $Y^Z$  and curvature-dependent yield terms  $S^{Z,\text{eros.}}$ ), and

also to the effects of redistributed atoms (via the terms  $S^{Z,\text{redist.}}$ ). Although it applies only to the height field, and our aim here is to estimate the behavior of multi-component theories, we now have sufficient information to estimate several parameters within these theories. By carefully examining the equation for the height field in any given two-component theory, we can identify the associated terms, and equate the coefficients in Eq.(15) with *underlying parameter groups* in the theory. These underlying parameter groups, in turn, will allow us to estimate several of the coefficients in equations (2)-(3). Although this approach defies a single mathematical notation due to differences between theories, it is straightforward, and we shall now offer a lengthy demonstration for an important example problem.

#### IV. AN EXAMPLE APPLICATION: IRRADIATED BINARY ALLOYS

We now present an application of the general method described above to the regime of irradiated binary alloys. The most detailed coupled-PDE theory for this system is that of Bradley and Shipman [13, 14], which generalizes earlier work of Shenoy, Chan, and Chason [12] to include the effect of both net and preferential redistribution of atoms that are not sputtered away from the surface – i.e., the so-called Carter-Vishnyakov effect [23]. Although it is a general framework applicable to the irradiation of any binary material, the work of Bradley and Shipman had primarily in mind the irradiation of GaSb, where ordered hexagonal dot structures were famously first observed [1]. We therefore illustrate how one may use molecular dynamics simulations to estimate the value of parameters in the theory for GaSb. (Note: when referring to specific equations within the BS theory, we refer to the longer and more detailed Ref. [14], despite the earlier publication of Ref. [13]).

##### A. The Bradley-Shipman Theory and Connection with Crater Functions

The Bradley-Shipman theory starts from Eqs.(2)-(3), and applies the simplifying assumption that one can neglect the terms  $B\nabla^2 c$  in Eq.(2) and  $D'\nabla^4 h$  in Eq.(3) due to equal mobilities of target atoms. We deviate slightly from Ref.[14] by assuming that species  $A$  is preferentially sputtered (rather than species  $B$ ), and define coefficients in such a way that zeroth- and fourth-order terms in Eqs.(2)-(3) have negative sign, whereas second-

order terms have positive sign. The coefficients in Eq.(2) for the height evolution are then defined via

$$\begin{aligned}
A &= P_0 \Omega [\Lambda'_A (c_{A,0}) - \Lambda'_B (c_{B,0})] \\
C &= \Omega [(\mu_A (c_{A,0}) + \mu_B (c_{B,0})) - \alpha (\Lambda_A (c_{A,0}) + \Lambda_B (c_{B,0}))] \\
D &= [c_{A,0} D_A + c_{B,0} D_B] \frac{n_s \Omega^2 \gamma_s}{k_B T} > 0
\end{aligned} \tag{17}$$

and in Eq.(3) for the concentration evolution, via

$$\begin{aligned}
A' &= \frac{P_0 \Omega}{\Delta} [c_{B,b} \Lambda'_A (c_{A,0}) + c_{A,b} \Lambda'_B (c_{B,0})] > 0 \\
B' &= \frac{n_s \Omega}{\Delta} [c_{B,b} D_A + c_{A,b} D_B] > 0 \\
C' &= \frac{\Omega}{\Delta} [c_{B,b} \mu_A (c_{A,0}) - c_{A,b} \mu_B (c_{B,0})]
\end{aligned} \tag{18}$$

Here  $P_0$  is the power deposited by the ions per unit surface area on a flat surface,  $\Omega$  is the atomic volume (taken to be the same for both species),  $n_s$  is the total number of mobile surface atoms per unit area on the surface,  $\gamma_s$  is the surface energy,  $k_B$  is Boltzmann's constant,  $T$  is the temperature,  $\Delta$  is the amorphous film thickness,  $c_{A,0}$  and  $c_{B,0}$  are the concentration of  $A$  and  $B$  atoms in the film at steady state,  $c_{A,b}$  and  $c_{B,b}$  are the concentration of  $A$  and  $B$  atoms in the bulk,  $D_A$  and  $D_B$  are the diffusivities of  $A$  and  $B$  atoms,  $\Lambda_A (c_A)$  and  $\Lambda_B (c_B)$  are proportionality constants linking the deposited power to the sputtering rate, and  $\mu_A (c_A)$  and  $\mu_B (c_B)$  are proportionality constants describing preferential redistribution of material, an effect first proposed in Refs.[13, 14] and playing a critical role therein.

To connect with the results of Section III, the key equation in the Bradley-Shipman theory is Eq.(7) of Ref.[14], with additional definitions provided by Eqs.(3)-(6) therein. Combining those four equations, one obtains an evolution equation for the height field of

$$\frac{\partial h}{\partial t} = -\Omega P_0 (\Lambda_{A,0} + \Lambda_{B,0}) + \Omega (-\alpha \Lambda_{A,0} - \alpha \Lambda_{B,0} + \mu_A + \mu_B) \nabla^2 h + \dots, \tag{19}$$

where all terms directly due to ion-bombardment are present, and terms related to diffusive processes are omitted. Upon comparison of Eq.(19) with Eq.(15), it can easily be seen that there is a one-to-one correspondence between the coefficients of the two equations,

and the physical effect underlying each. Although these equations were obtained by different means, they describe precisely the same physical mechanisms. We therefore equate them in a term-by-term manner for the case of normal incidence ( $\theta = 0$ ), obtaining

$$\begin{aligned}
\Omega_A P_0 \Lambda_{A,0} &= -Y^A \\
\Omega_B P_0 \Lambda_{B,0} &= -Y^B \\
\Omega_A \alpha \Lambda_{A,0} &= -S_{X,Y}^{A,\text{eros.}} \\
\Omega_B \alpha \Lambda_{B,0} &= -S_{X,Y}^{B,\text{eros.}} \\
\Omega_A \mu_{A,0} &= S_{X,Y}^{A,\text{redist.}} \\
\Omega_B \mu_{B,0} &= S_{X,Y}^{B,\text{redist.}}
\end{aligned} \tag{20}$$

Finally, combining the relationships (20) with the definitions for  $\{A, C, A', C'\}$  in Eqs.(17)-(18), we can then estimate these parameters as follows

$$\begin{aligned}
A &= -\left([Y^A]' - [Y^B]'\right) \\
C &= \left(c_{A,0} S_{X,Y}^{A,\text{eros.}} + c_{B,0} S_{X,Y}^{B,\text{eros.}} + c_{A,0} S_{X,Y}^{A,\text{redist.}} + c_{B,0} S_{X,Y}^{B,\text{redist.}}\right) \\
A' &= -\frac{1}{\Delta} \left(c_{A,b} [Y^B]' + c_{B,b} [Y^A]'\right) > 0 \\
C' &= \frac{1}{\Delta} \left(c_{B,b} c_{A,0} S_{X,Y}^{A,\text{redist.}} - c_{A,b} c_{B,0} S_{X,Y}^{B,\text{redist.}}\right)
\end{aligned} \tag{21}$$

We see that fully four out of six of the BS parameters are accessible to MD studies. As we anticipated in Section II C, these happen to be precisely the parameters that govern the behavior of the longest wave perturbations to the surface height, via the finite-wavelength requirement in Eq.(11). Thus, the results of MD simulation may be used to predict whether an irradiated binary system should have long-wave or finite-wavelength instabilities, a surprising result that allows the prediction of a key distinguishing characteristic of pattern-forming systems.

## B. Simulation Environment and Initial Results

Using molecular dynamics simulations, we have performed simulations of GaSb irradiated by Ar ions at 250 eV. The simulations were carried out with the PARCAS code [32], following similar general principles for surface irradiation simulations as presented earlier

in Refs. [33, 34]. The same simulation approach has earlier been shown to give reasonable agreement with experimental sputtering yields in Si [35]. Amorphous GaSb was created by annealing a cubic piece of initially crystalline GaSb, consisting of  $1.1 \times 10^4$  atoms. In these simulations periodic boundary conditions were used. Copies of the obtained amorphous GaSb were joined together (3 in the  $x$ - and  $y$ -directions, and 2 in the  $z$ -direction) to form a target consisting of nearly  $2.0 \times 10^5$  atoms. Finally, the target was cleaved in the  $z$ -direction, and the resulting free surface was relaxed at 0 K, with periodicity only in the  $x$ - and  $y$ -directions.

The inter-atomic potentials used for Ga-Sb interactions was that of Powell et al [36]. The (rarely occurring) pure Ga interactions were the same as those in the GaAs potential developed by us [37]. To obtain the Sb potential, we note that As and Sb have the same crystal structure. Hence, the As potential parameter  $D_e$  [37] was rescaled with the difference in cohesive energies of the two elements, and the parameter  $r_0$  with the difference in lattice constants. This gave a cohesive energy of 2.72 eV/atom and a density of  $7.28 \text{ g/cm}^3$  for pure Sb, in reasonable agreement with the experimental values of 2.72 eV/atom and  $6.74 \text{ g/cm}^3$ . We emphasize that since regions of pure Ga or Sb should not form in the simulated system, the results are not expected to be sensitive to small inaccuracies in the description of the pure elements.

For each different irradiation angle, we simulated 300 independent Ar ion impacts onto the target just constructed. Each ion hit the target at a random location, and for off normal incidence, arrived from a random azimuthal angle. Periodic boundary conditions were used in the  $x$  and  $y$  directions, with a thermostat dynamically applied to vertical and horizontal strips of material halfway across the cell from the impact position, so as to form cooled walls within which the impact was centered. Together with a thermostat layer at the bottom of the cell, these served to remove energy from the system over time. The simulation time of each impact was 250 ps, which is rather long, but turned out to be necessary for the post-impact atomic movements to seize.

As discussed in Ref.[19], two sources of noise were then filtered from the data before the moments were measured. First, despite the careful preparation of the target, some residual stresses remain, leading to displacements during the simulation that are due to the pre-existing state of the target, rather than to the impact. Second, the periodic nature

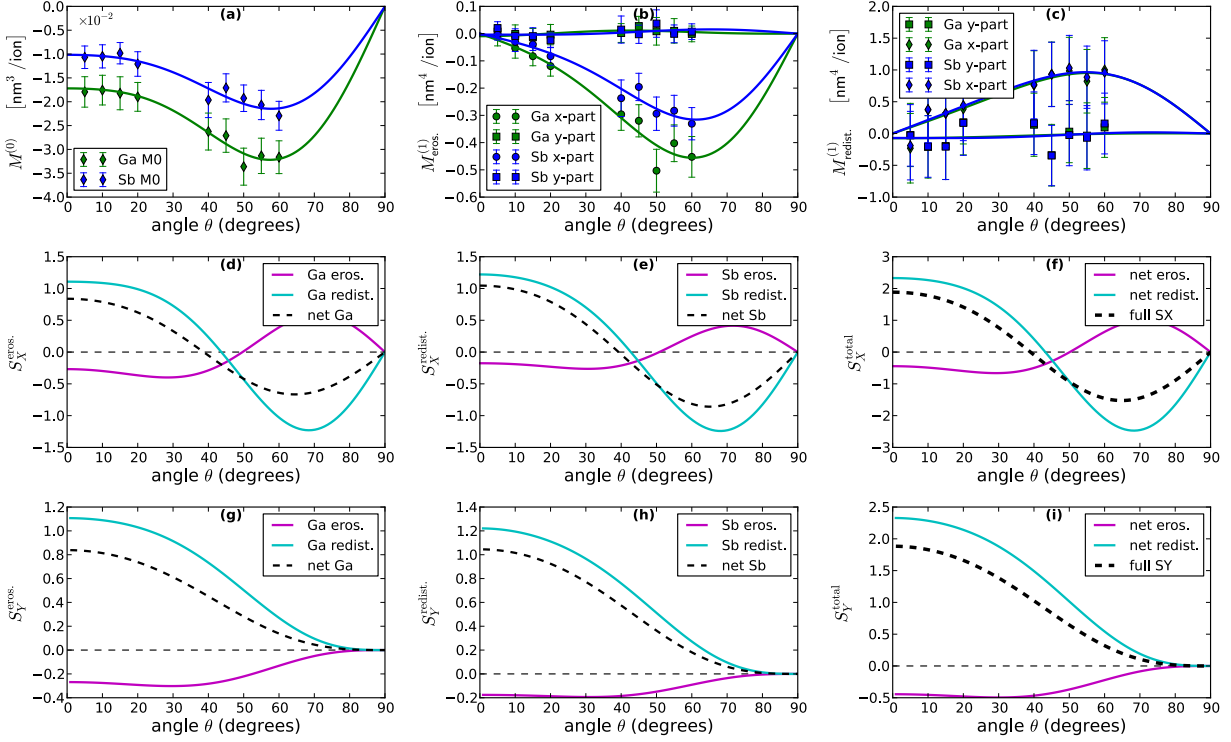


Figure 2. Moments and coefficients by component. (a-c) The zeroth moment  $M^{(0)}$ , the first erosive moment  $M_{\text{eros.}}^{(1)}$ , and the first redistributive moment  $M_{\text{redist.}}^{(1)}$ ; decomposed into contributions from Ga and Sb. These plots indicate that Ga is preferentially sputtered from a homogeneous, amorphous film at 50/50 initial concentrations, but that both species are redistributed approximately equally. (d-f) The erosive and redistributive contribution to  $S_X$  for each species separately, and summed over both species. (g-i) The corresponding plots for  $S_Y$  (for completeness only - at  $\theta = 0$  both values are equal). It is readily seen that the contributions of erosion and redistribution have the same relative shapes and sizes for each species, with the redistributive component playing the dominant role at most angles. Note that while the full angle-dependence of the curves in (d-i) is estimated for illustrative purposes, our concern here is only with the values at  $\theta = 0$ .

of the cell allows small coherent shears to occur, on the scale of the entire cell. These are both filtered by constructing an annulus around the impact cite, and calculating both the average lab-frame displacement of each atom, as well as the average shear in a co-ordinate system aligned with the incoming ion direction. Both averages were then subtracted from the displacement field, after which moments were calculated according to Eq.(14).

The results of our simulations are shown in Fig.2. We first calculate the moments according to Eq.(14), at nine different angles, and plot them along with three-term Fourier fits. For comparison with the normal-incidence irradiation conditions of the Bradley-Shipman theory, our primary interest is in the simulations near  $\theta = 0$ . However, additional data at intermediate angles is also provided for general reference, and these, along with symmetry considerations at  $\theta = 90$ , improve the quality of the fits (see Ref.[19] for more details). Our Fig. 2a indicates that, for an initial fresh, unsegregated 50/50 target, Ga is preferentially sputtered relative to Sb, and consequently exhibits a stronger curvature dependent sputtering effect in Fig. 2b (see Section IV E below for a discussion of this result). In contrast, the strikingly similar shape of the curves in Fig. 2c suggests that preferential redistribution is unlikely to be a significant effect for this system. A comparison of the relative magnitudes of the curves in Figures 2b and 2c suggests that redistribution will overwhelm the effect of erosion, as has been seen in pure materials.

To confirm that these impressions are not altered under the derivatives in Eqs.(16), and to obtain exactly the coefficients required by Eq.(20) for comparison with the BS theory, we also plot the coefficients found in that equation in Figures 2d-i. Here we compare the erosive and redistributive contributions to both  $S_X$  and  $S_Y$  for each atomic species separately, and the net erosive and redistributive contributions summed over both species. We confirm that the redistributive contributions are dominant, and we also note the striking similarity of the shapes of the curve for each species, which are also similar to the shapes observed in pure silicon [19]. This indicates that chemical composition is not a strong influence on the collision cascade in a homogeneous target, suggesting that the dominance of redistribution may potentially be a generic feature of low-energy ion bombardment.

Using the data shown in Figure 2, and the definitions of the coefficients from Eqs.(16), we now proceed to obtain the values of the coefficients of Equation (15)



$$\begin{aligned}
Y^{\text{Ga}} &= -0.0172 \times I_0 \frac{\text{nm}}{\text{s}} \\
Y^{\text{Sb}} &= -0.0102 \times I_0 \frac{\text{nm}}{\text{s}} \\
S_{X,Y}^{\text{Ga,eros.}} &= -0.269 \times I_0 \frac{\text{nm}^2}{\text{s}} \\
S_{X,Y}^{\text{Sb,eros.}} &= -0.176 \times I_0 \frac{\text{nm}^2}{\text{s}} \\
S_{X,Y}^{\text{Ga,redist.}} &= 1.11 \times I_0 \frac{\text{nm}^2}{\text{s}} \\
S_{X,Y}^{\text{Sb,redist.}} &= 1.22 \times I_0 \frac{\text{nm}^2}{\text{s}}
\end{aligned} \tag{22}$$

where all coefficients are estimated at  $\theta = 0$  and  $c_A = c_B = 0.5$ , and where  $I_0$  is again the flux in the beam direction, as in Eq.(16).

### C. Extrapolation to Steady Concentration

The final step in estimating the coefficients  $\{A, C, A', C'\}$  is to observe that the various components of the moments  $M^{(0)}$  and  $M^{(1)}$  are functions not only of angle, but also of the concentrations of the various species within the target. Similarly, within the BS theory, the quantity  $\Lambda_i$  - associated with sputter yield - and presumably also  $\mu_i$  - describing the redistributive flux - share this dependence. [The latter dependence was not discussed in Ref.[14], but presumably exists.] In both Equations (20) and (21), therefore, all coefficients  $Y$  and  $S$  must in principle be evaluated at the steady-state concentration  $(c_{A,0}, c_{B,0})$ . The steady concentration, in turn, depends implicitly upon the relative shapes of the yield functions  $\Lambda_A(c_A)$  and  $\Lambda_B(c_B)$ , as specified in Eq. (12) of Ref.[14]. This presents a challenge to a molecular dynamics investigation, because in addition to the simulations over many angles described here, one would also have to perform simulations over many different target compositions. This, in turn, requires constructing many different targets, which is actually the most time-consuming step.

Because of these considerations, and limited computational capacity, we are led to make an important simplifying assumption. We will assume that each species both sputters and redistributes at a rate linearly proportional to its concentration in the film (c.f. Refs. [15, 16]), with rate zero when its concentration is zero, and rate equal to our measured

rate when its concentration is one half. This gives, for the moments,

$$\begin{aligned} M_Z^{(0)}(c_Z) &= M_Z^{(0)}\left(\frac{1}{2}\right) \times (2c_Z) \\ M_{Z,\text{type}}^{(1)}(c_Z) &= M_{Z,\text{type}}^{(1)}\left(\frac{1}{2}\right) \times (2c_Z) \end{aligned} \quad (23)$$

and for the corresponding assumption on the coefficients,

$$\begin{aligned} Y^Z(c_Z) &= Y^Z\left(\frac{1}{2}\right) \times 2c_Z \\ S^{Z,\text{type}}(c_Z) &= S^{Z,\text{type}}\left(\frac{1}{2}\right) \times 2c_Z \end{aligned} \quad (24)$$

Under this assumption, we will be able both to estimate the steady concentration, and also estimate coefficients at that concentration, without excessive numerical simulation (see Section IV E below for further discussion).

Under the assumptions (23) and (24), and using Eq. (12) of Ref.[14], the values in Eq.(20) for  $Y^{\text{Ga}}$  and  $Y^{\text{Sb}}$  predict steady concentrations of Ga and Sb to be

$$\begin{aligned} c_{\text{Ga},0} &= 0.37 \\ c_{\text{Sb},0} &= 0.63 \end{aligned}$$

Then, combining the estimates (22) at the 50/50 concentration with the assumption (24) on the concentration dependence of the coefficients, we use expression (21) to produce final estimates for  $\{A, C, A', C'\}$  of

$$\begin{aligned} A &\approx 0.014 \times I_0 \frac{\text{nm}}{\text{s}} \\ C &\approx 1.9 \times I_0 \frac{\text{nm}^2}{\text{s}} \\ A' &\approx .0091 \times I_0 \frac{1}{\text{s}} \\ C' &\approx -.12 \times I_0 \frac{\text{nm}}{\text{s}} \end{aligned} \quad (25)$$

where we have estimated the value  $\Delta \approx 3 \text{ nm}$  from TEM measurements of pure silicon irradiated at the same 250 eV [38].

## D. Discussion

A major accomplishment of the Bradley-Shipman theory was its identification of a narrow band of unstable wavenumbers in the Equations (2)-(3), bounded both above and below by stable wavenumbers. As described in Section II C, this is the essential first ingredient for producing highly-ordered patterns of any kind, and the BS theory was the first physically-derived theory to admit this kind of instability. However, to do so it placed quite severe requirements on the parameters in the model.

We quickly summarize these constraints by recalling the generic dispersion relation

$$\sigma_+(k) = \frac{1}{2} \left( -\tau + \sqrt{\tau^2 - 4\Delta} \right). \quad (26)$$

and the coefficients defined in the BS theory

$$\tau(k) = A' + (C + B')k^2 + Dk^4 \quad (27)$$

$$\Delta(k) = (CA' - AC')k^2 + (CB' + DA')k^4 + (DB')k^6. \quad (28)$$

Now, a general feature of Eq.(26) is that a mode is only unstable if either  $\tau < 0$  or  $\Delta < 0$  [25]. As described above, a narrow band of unstable modes requires stable longwaves, which in turn requires that  $(CA' - AC') > 0$ . Then, because the parameters  $D$ ,  $A'$ , and  $B'$  are all positive, we see that the only way to achieve  $\tau < 0$  or  $\sigma < 0$  is if (a) the coefficient  $C$  is sufficiently negative to drive the instability, which in turn requires that (b) the parameter group  $AC'$  is sufficiently negative to stabilize the long waves, with  $|AC'| > |A'C|$ . These were striking requirements of the Bradley-Shipman instability, as the former requirement, in particular, is contrary to results for pure Silicon and Germanium [39, 40], where  $C > 0$  due to the dominance of redistributive over erosive effects [19].

Indeed, as we have shown here, (1) the positive value of  $C$  persists in the case of binary GaSb, in a way that suggests this may be a generic feature of low-energy ion irradiation; (2) the parameter group  $AC'$  in Eq.(8) (the only place that either  $A$  or  $C'$  occur in the BS theory) is much smaller in magnitude than the similarly-dimensioned group  $A'C$ , suggesting that preferential redistribution is likely not an important effect. These findings are contrary to the requirements of the Bradley-Shipman theory - in fact, because both  $C$  and

$(A'C - C'A)$  were found to be positive, and because  $D$ ,  $A'$ , and  $B'$  are positive by definition, the BS theory should predict stable, flat surfaces for normal-incidence irradiation of GaSb, in contrast to the dot-like patterns seen experimentally.

### E. Limitations.

We want to acknowledge the following limitations of the MD simulations performed in Section IVB, due to finite computational resources in the simulation stage. Although they are not an inherent limitation of the general approach described in Section III, they provide directions for future improvement of our estimates.

First, the definitions for the coefficients  $Y^Z$  and  $S^{Z,\text{type}}$  in Eq.(16), like the corresponding definitions in Ref.[19] from which they are generalized, are the result of performing simulated impacts on an initially flat target surface. As such, they represent simplifications of the more general results in Ref.[18] for arbitrary curved surfaces. Obtaining such generalized results would, unfortunately, require simulation of impacts not only over many angles, but also on many different types of curved surface, which is outside our current computational capacity. Although this simplification may change the absolute magnitude of the identified coefficients, it does not significantly change the relative magnitudes, upon which our conclusions are entirely based.

Second, our simulations were performed only at the 50/50 concentration for a fresh, homogeneous target. We have estimated values of coefficients at the steady concentration by means of the linear approximations in Eqs. (23)-(24), as exemplified in a similar context [16]. Like the flat-surface simplification, this avoids the simulation of targets at a variety of concentrations. With more computational resources, such simulations could of course be performed, which would improve upon the accuracy of the estimates. However, in addition to the computational cost of the simulations themselves, this would require the construction of many targets, which is in fact the most time-consuming part of our study. In addition, the nature of the irradiated target away from the 50/50 concentration is not currently well-known.

Third, our results indicating that Ga is sputtered preferentially relative to Sb for a fresh, unsegregated target at the 50/50 concentration do not agree with early observations of

significant Ga *enrichment* at the surface [41], even (to a lesser extent) in the absence of oxygen which preferentially oxidizes Ga at the surface [21, 42, 43]. Because of the disagreement with experiment, we also performed simulations in SDTrimSP (**author?**) [44]. For a variety of inter-atomic potentials, these simulations were roughly consistent with the results from MD, with around a 10% preferential yield of Ga at the 50/50 composition, and a significantly higher yield of pure Ga than for pure Sb. These atomistic results are all consistent with the more efficient energy transfer of Ar to Ga relative to the heavier Sb. It is therefore likely that experimental target conditions differ from the ones in typical atomistic targets in ways that still need to be carefully understood. For instance, although the methods used to produce amorphous GaSb discussed above result in an approximately homogeneous target, in Refs.[43, 45] it was found that the lower vacuum surface energy of Sb may pull these atoms preferentially to the top monolayer of the target via Gibbsian segregation, resulting in a surface layer enriched with Sb above a subsurface layer enriched with Ga. It is easy to speculate that such a configuration may lead to enhanced sputtering of Sb relative to an unsegregated target, and preliminary SDTrimSP simulations suggest that this could readily promote Sb to be the preferentially sputtered species. In any case, it is clear that future work to bring the simulated results into agreement with experiment will require a better understanding of precisely what is happening during the early stages of irradiation, and the construction of an atomistic target reflecting that understanding.

Despite the limitations just described, we anticipate that our two principal conclusions for the GaSb system are likely to remain valid as more accurate targets are developed. In particular, although the relative response of Ga vs. Sb atoms might well be altered by surface segregation, it is more doubtful that the relative response of eroded vs redistributed atoms would be so altered – Figure 2 demonstrates that redistribution overwhelms erosion for each species *individually*, precisely as observed in pure Silicon at similar energies [19]. Therefore, the contributions to the sign of  $C$  are positive *for both species*, and changing the relative amount of Ga and Sb in the target would not change the sign of this parameter. Regarding the relative importance of preferential redistribution, the parameters  $A$  and  $C'$  - which depend on *differential* erosion and redistribution - may be expected to vary somewhat for different target structures. However, these only appear as the product  $AC'$ , which only appears together with the group  $A'C$ . The latter group depends only on *net*

erosion and redistribution, and should therefore be altered much less by compositional changes. Because this latter group was found to be ten times larger than the former, we suspect that even improved estimates with better targets would be unlikely to reverse the relative sizes of these terms.

## V. CONCLUSIONS

We have shown that many parameters of coupled PDE models for the irradiation of two-component materials may be estimated using Molecular Dynamics simulation by means of an extension, to binary materials, of the theory of crater functions described in [18, 19]. In principle, these include parameters describing net sputtering and redistribution ( $C$ ), preferential sputtering ( $A$ ), preferential redistribution ( $C'$ ), and material replenishment ( $A'$ ). Remarkably, these are exactly the four parameters needed to calculate the critical parameter group ( $A'C - C'A$ ), which governs the behavior of long waves in all such theories. The methods demonstrated here are general, and should therefore be applicable to a wide variety of coupled PDE models for irradiated binary systems [13, 14], enabling the prediction of this important distinguishing characteristic among a variety of pattern-forming systems.

Subsequently, we have performed the first estimate of these four parameters within the Bradley-Shipman theory of irradiated binary alloys, as applied to the low-energy irradiation of GaSb by Ar, in which hexagonal dot arrays were first observed. Our main finding for this system is that the parameter  $C$  is positive for normal incidence irradiation of GaSb, indicating the dominance of redistribution over erosion, as was predicted by MD for pure Si [19], and shown experimentally for both pure Si and Ge [39, 40]. Additionally, we saw that the parameter  $C'$  associated with preferential redistribution, hypothesized to be an important physical effect in ordered dot formation, appears too small to play an important role.

Both the positive value of  $C$ , and the relative unimportance of  $C'$ , are contrary to requirements of the Bradley-Shipman theory on the formation of well-ordered patterns. In fact, for the parameter values we have estimated, that theory would predict entirely smooth surfaces for low-energy, normal-incidence irradiation of GaSb. Especially if our

results extend to a wide range of other two-component materials (in other words, if they are a generic property of the kinetically-dominated collision cascade for low energy irradiation), then these findings provide strong motivation for the consideration of alternative physical mechanisms to explain the ordered patterns observed in these systems. We investigate such a mechanism elsewhere [46].

---

- [1] S. Facsko, T. Dekorsy, C. Koerdt, C. Trappe, H. Kurz, A. Vogt, H. L. Hartnagel, Formation of ordered nanoscale semiconductor dots by ion sputtering, *Science* 285 (1999) 1551–1553. doi:DOI:10.1126/science.285.5433.1551.
- [2] W. L. Chan, E. Chason, Making waves: kinetic processes controlling surface evolution during low energy ion sputtering, *J. Appl. Phys.* 101 (2007) 121301. doi:10.1063/1.2749198.
- [3] R. Gago, L. Vásquez, O. Plantevin, T. H. Metzger, J. Muñoz-García, R. Cuerno, M. Castro, Order enhancement and coarsening of self-organized silicon nanodot patterns induced by ion-beam sputtering, *Appl. Phys. Lett.* 89 (2006) 233101. doi:10.1063/1.2398916.
- [4] F. Frost, B. Ziberi, A. Schindler, B. Rauschenbach, Surface engineering with ion beams: From self-organized nanostructures to ultra-smooth surfaces, *Appl. Phys. A* 91 (2008) 551–559. doi:10.1007/s00339-008-4516-0.
- [5] B. Ziberi, F. Frost, M. Tartz, H. Neumann, B. Rauschenbach, Ripple rotation, pattern transitions, and long range ordered dots on silicon by ion beam erosion, *Appl. Phys. Lett.* 92 (2008) 063102.
- [6] G. Ozaydin, A. Ozcan, Y. Wang, K. Ludwig, H. Zhou, R. Headrick, D. Siddons, Real-time x-ray studies of Mo-seeded Si nanodot formation during ion bombardment, *Applied Physics Letters* 87 (2005) 163104.
- [7] G. Ozaydin, J. K. F. Ludwig, H. Zhou, R. L. Headrick, Effects of mo seeding on the formation of si nanodots during low-energy ion bombardment, *J. Vac. Sci. Technol. B* 26 (2008) 551. doi:10.1116/1.2870222.
- [8] G. Ozaydin-Ince, K. F. Ludwig Jr., In situ x-ray studies of native and mo-seeded surface nanostructuring during ion bombardment of si(100), *J. Phys. Cond. Matt.* 21 (2009) 224008.
- [9] S. Macko, F. Frost, B. Ziberi, D. Forster, T. Michely, Is keV ion-induced pattern formation on

- Si(001) caused by metal impurities?, *Nanotechnology* 21 (2010) 085301.
- [10] K. Zhang, M. Brötzmann, H. Hofsäas, Surfactant-driven self-organized surface patterns by ion beam erosion, *New Journal of Physics* 13 (2011) 013033. doi:10.1088/1367-2630/13/1/013033.
- [11] C. S. Madi, M. J. Aziz, Multiple scattering causes the low energy-low angle constant wavelength bifurcation of argon ion bombarded silicon surfaces, *Applied Surface Science* 258 (2012) 4112–4115, (IINM2011 Bhubaneswar Conference Proceedings).
- [12] V. B. Shenoy, W. L. Chan, E. Chason, Compositionally modulated ripples induced by sputtering of alloy surfaces, *Physical Review Letters* 98 (2007) 256101.
- [13] R. M. Bradley, P. D. Shipman, Spontaneous pattern formation induced by ion bombardment of binary compounds, *Physical Review Letters* 105 (2010) 145501.
- [14] P. D. Shipman, R. M. Bradley, Theory of nanoscale pattern formation induced by normal-incidence ion bombardment of binary compounds, *Physical Review B* 84 (2011) 085420.
- [15] R. M. Bradley, Surface instability of binary compounds caused by sputter yield amplification, *Journal of Applied Physics* 111 (2012) 114305. doi:10.1063/1.4724342.
- [16] R. M. Bradley, Theory of nanodot and sputter cone arrays produced by ion sputtering with concurrent deposition of impurities, *Physical Review B* 83 (2011) 195410.
- [17] G. Abrasonis, K. Morawetz, Instability types at ion-assisted alloy deposition: from two-dimensional to three-dimensional nanopattern growth, *Physical Review B* 86 (2012) 085452. doi:10.1103/PhysRevB.86.085452.
- [18] S. A. Norris, M. P. Brenner, M. J. Aziz, From crater functions to partial differential equations: A new approach to ion bombardment induced nonequilibrium pattern formation, *J. Phys. Cond. Matt.* 21 (2009) 224017. doi:10.1088/0953-8984/21/22/224017.
- [19] S. A. Norris, J. Samela, L. Bukonte, M. Backman, D. F. K. Nordlund, C. Madi, M. Brenner, M. Aziz, Molecular dynamics of single-particle impacts predicts phase diagrams for large scale pattern formation, *Nature Communications* 2 (2011) 276.
- [20] S. Le Roy, E. Søndergård, I. S. Nerbø, M. Kildemo, M. Plapp, Diffuse-interface model for nanopatterning induced by self-sustained ion-etch masking, *Physical Review B* 81 (2010) 161401(R).
- [21] O. El-Atwani, J. P. Allain, A. Cimaroli, A. Suslova, S. Ortoleva, The significance of in situ



- conditions in the characterization of gasb nanopatterned surfaces via ion beam sputtering, *Journal of Applied Physics* 110 (2011) 074301. doi:10.1063/1.3642997.
- [22] R. M. Bradley, J. M. Harper, Theory of ripple topography induced by ion bombardment, *J. Vac. Sci. Technol.* 6 (1988) 2390–2395.
- [23] G. Carter, V. Vishnyakov, Roughening and ripple instabilities on ion-bombarded si, *Phys. Rev. B* 54 (1996) 17647–17653. doi:10.1103/PhysRevB.54.17647.
- [24] B. P. Davidovitch, M. J. Aziz, M. P. Brenner, On the stabilization of ion sputtered surfaces, *Phys. Rev. B* 76 (2007) 205420. doi:10.1103/PhysRevB.76.205420.
- [25] M. Cross, H. Greenside, *Pattern Formation and Dynamics in Nonequilibrium Systems*, Cambridge University Press, 2011, iISBN: 0521770505.
- [26] M. Castro, R. Cuerno, Hydrodynamic approach to surface pattern formation by ion beams, *Applied Surface Science* 258 (2012) 4171–4178. doi:10.1016/j.apsusc.2011.09.008.
- [27] S. A. Norris, Stress-induced patterns in ion-irradiated silicon: model based on anisotropic plastic flow, *Phys. Rev. B* 86 (2012) 235405, arxiv:1207.5754.
- [28] M. Castro, R. Gago, L. Vázquez, J. Muñoz-García, R. Cuerno, Stress-induced solid flow drives surface nanopatterning of silicon by ion-beam irradiation, *Physical Review B* 86 (2012) 214107.
- [29] W. W. Mullins, Flattening of a nearly plane solid surface due to capillarity, *J. Appl. Phys.* 30 (1959) 77.
- [30] S. E. Orchard, On surface levelling in viscous liquids and gels, *Appl. Sci. Res.* 11A (1962) 451.
- [31] C. C. Umbach, R. L. Headrick, K.-C. Chang, Spontaneous nanoscale corrugation of ion-eroded SiO<sub>2</sub>: The role of ion-irradiation-enhanced viscous flow, *Phys. Rev. Lett.* 87 (2001) 246104. doi:10.1103/PhysRevLett.87.246104.
- [32] K. Nordlund, PARCAS computer code. The main principles of the molecular dynamics algorithms are presented in [34, 47]. The adaptive time step and electronic stopping algorithms are the same as in [48] (2010).
- [33] J. Tarus, K. Nordlund, A. Kuronen, J. Keinonen, Effect of surface on defect creation by self-ion bombardment of si (001), *Phys. Rev. B* 58 (1998) 9907.
- [34] M. Ghaly, K. Nordlund, R. S. Averback, Molecular dynamics investigations of surface damage produced by kiloelectronvolt self-bombardment of solids, *Philos. Mag. A* 79 (1999) 795–820.

- [35] J. Samela, K. Nordlund, J. Keinonen, V. N. Popok, Comparison of silicon potentials for cluster bombardment simulations, *Nucl. Inst. Meth. Phys. Res. B* 255 (2007) 253–258.
- [36] D. Powell, M. A. Migliorato, A. G. Cullis, Optimized tersoff potential parameters for tetrahedrally bonded iii-v semiconductors, *Phys. Rev. B* 75 (11) (2007) 115202.
- [37] K. Albe, K. Nordlund, R. S. Averback, Modeling metal-semiconductor interaction: Analytical bond-order potential for platinum-carbon, *Phys. Rev. B* 65 (2002) 195124.
- [38] C. S. Madi, Linear stability and instability patterns in ion bombarded silicon surfaces, Ph.D. thesis, Harvard University (2011).
- [39] C. S. Madi, E. Anzenberg, K. F. Ludwig Jr., , M. J. Aziz, Mass redistribution causes the structural richness of ion-irradiated surfaces, *Phys. Rev. Lett.* 106 (2011) 066101.
- [40] E. Anzenberg, J. C. Perkinson, C. S. Madi, M. J. Aziz, K. F. Ludwig Jr., Nanoscale surface pattern formation kinetics on germanium irradiated by  $kr^+$  ions, *Phys. Rev. B* 86 (2012) 245412.
- [41] S. Le Roy, E. Barthel, N. Brun, A. Lelarge, E. Søndergård, Self-sustained etch masking: A general concept to initiate the formation of nanopatterns during ion erosion, *Journal of Applied Physics* 106 (2009) 094308.
- [42] O. El-Atwani, J. P. Allain, A. Suslova, The effect of native oxide on ion-sputtering-induced nanostructure formation on gasb surfaces, *Applied Physics Letters* 101 (2012) 251606.
- [43] O. El-Atwani, J. P. Allain, S. Ortoleva, In-situ probing of near and below sputter-threshold ion-induced nanopatterning on GaSb(1 0 0), *Nuclear Instruments and Methods in Physics Research B* 272 (2012) 210–213.
- [44] A. Mutzke, R. Schneider, W. Eckstein, R. Dohmen, SDTrimSP version 5.0, IPP Report 12/8, Garching (2011).
- [45] W. Yu, J. L. Sullivan, S. S. O., Xps and leiss studies of ion bombarded gasb, insb and cdse surfaces, *Surface Science* 352–354 (1996) 781–787.
- [46] S. A. Norris, A chemically-driven finite-wavelength instability in ion-irradiated compound semiconductors, arXiv:1205.6834v1 [cond-mat.mtrl-sci] (2013).
- [47] K. Nordlund, M. Ghaly, R. S. Averback, M. Caturla, T. D. de la Rubia, J. Tarus, Defect production in collision cascades in elemental semiconductors and fcc metals, *Phys. Rev. B* 57 (1998) 7556–7570.

- [48] K. Nordlund, Molecular dynamics simulation of ion ranges in the 1 – 100 keV energy range, *Comput. Mater. Sci.* 3 (1995) 448.